Photoelectrochemistry Hot Paper

DOI: 10.1002/anie.201403611

Formation of Mesoporous Heterostructured $BiVO_4/Bi_2S_3$ Hollow Discoids with Enhanced Photoactivity**

Xuehui Gao, Hao Bin Wu, Lingxia Zheng, Yijun Zhong, Yong Hu, and Xiong Wen (David) Lou**

Abstract: *Semiconductor heterostructures are of great interest in a wide range of applications. In this work, we design and synthesize a novel heteronanostructure with controlled relative composition, i.e., $BiVO_4/Bi_2S_3$ hollow discoid-like particles with mesoporous shell. The synthesis involves a facile anion exchange process by reacting pre-synthesized $BiVO_4$ discoid-like particles with Na_2S in an aqueous solution. Benefiting from the unique structural features and the formation of heterostructure, the as-prepared $BiVO_4/Bi_2S_3$ hollow discoids exhibit significantly enhanced photoelectrochemical current response and photocatalytic activity for reduction of Cr^{VI} under visible-light illumination.*

Semiconductor heterostructures usually exhibit enhanced or new physicochemical properties, which make them promising candidates for various applications with practical significance.[1] For example, semiconductor hybrid nanostructures with a staggered alignment of band edges at the heterointerface can improve spatial charge separation of photogenerated electrons and holes in different parts of the heterostructure, thus enhancing the photocatalytic and photovoltaic performance.[2–7] Moreover, hybrid materials with mesoporous structures or hollow interiors have received more attention compared to their solid counterparts because of their high specific surface area and enhanced ability to absorb light, thus acting as excellent photocatalysts for water and air purification.[8–9] To date, there have been several successes in the preparation of mesoporous hollow semiconductor heterostructures.[10–13] However, some inherent limitations in conventional synthesis methods, such as incompatibility between various materials, usually result in poor structural stability and uniformity of the synthesized heterostructures.[14] Therefore, it is of great interest to develop reliable and controllable strategies for the preparation of tailored heterostructured nanomaterials. Recently, ion exchange has been utilized as an attractive approach for chemical transformation of inorganic nanostructured materials while largely preserving the morphologies and structures of the starting materials.[15–20] Compared to cationic species, the diffusion of anions is generally much slower owing to their larger size. By choosing the proper diffusion pairs, the discrepancy in diffusion rates of the two components could be utilized to generate interior voids based on mechanisms similar to the nanoscale Kirkendall effect, which allows one to precisely tune the structural complexity.[21–28]

Monoclinic scheelite bismuth vanadate (m-$BiVO_4$), with a narrow band gap of 2.4 eV, is an important visible-light responsive photocatalyst and has been widely used in photocatalytic evolution of O_2 and degradation of organic pollutants.[29–32] However, its practical applications are still hindered by the poor quantum yield due to rapid recombination of photogenerated electrons and holes.[33] Thus, $BiVO_4$-based semiconductor heterostructures have received increasing attention owing to their excellent photocatalytic activity as a result of extended photo-responsive range and increased electron–hole pair separation efficiency.[34–35] The combination of two semiconductors with different energy levels may form an ideal system with rapid photoinduced charge separation and decreased chance of recombination of electron–hole pairs by the synergetic effect. The enhanced photocatalytic efficiency could originate from the fast transfer of photogenerated electrons and holes from one semiconductor to the other.[36]

Herein, we report a facile anion exchange method to form heterostructured $BiVO_4/Bi_2S_3$ hollow discoids with a mesoporous shell, which involves treating uniform $BiVO_4$ discoid nanostructures in a Na_2S aqueous solution under hydrothermal conditions. Importantly, the content of the Bi_2S_3 phase in the hybrid structure can be easily tuned by varying the concentration of Na_2S in the solution during the anion exchange process. This facile synthesis strategy for the mesoporous $BiVO_4/Bi_2S_3$ hollow heterostructures is schematically depicted in Figure 1. Benefiting from the unique structural features, the as-prepared $BiVO_4/Bi_2S_3$ heteronanostructures exhibit significantly enhanced photocurrent response and photocatalytic activity for reduction of Cr^{VI} under visible-light illumination.

[*] X. Gao, L. Zheng, Prof. Y. Zhong, Prof. Y. Hu
Key Laboratory of the Ministry of Education for Advanced Catalysis Materials, Institute of Physical Chemistry
Zhejiang Normal University, Jinhua, 321004 (P.R. China)
E-mail: yonghu@zjnu.edu.cn
H. B. Wu, Prof. X. W. Lou
School of Chemical and Biomedical Engineering
Nanyang Technological University
62 Nanyang Drive, Singapore 637459 (Singapore)
E-mail: xwlou@ntu.edu.sg
davidlou88@gmail.com
Homepage: http://www.ntu.edu.sg/home/xwlou/

[**] Y.H. acknowledges financial support from the Natural Science Foundation of China (21171146) and Zhejiang Provincial Natural Science Foundation of China for Distinguished Young Scholars (LR14B010001). The authors thank Dr. Bin Liu (Nanyang Technological University) for the help in measuring the photoelectrochemical current response.

Supporting information for this article is available on the WWW under http://dx.doi.org/10.1002/anie.201403611.

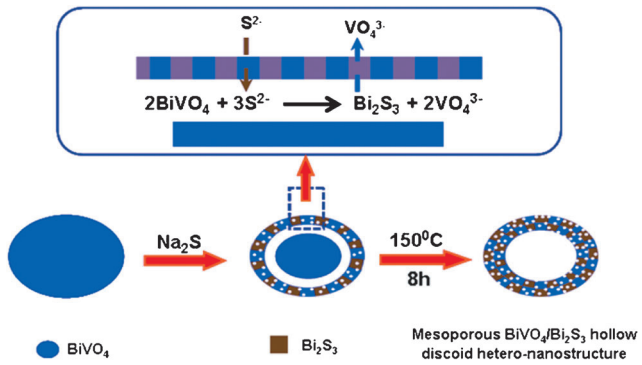

Figure 1. Formation of heterostructured $BiVO_4/Bi_2S_3$ hollow discoids with mesoporous shell by a controllable anion exchange process.

The precursor $BiVO_4$ discoids are prepared by a facile solvothermal method (see Experimental in the Supporting Information (SI)). The crystallographic structure and phase purity of the as-obtained sample are first examined by powder X-ray diffraction (XRD) analysis (Figure S1, see SI). All the diffraction peaks can be indexed as the body-centered monoclinic phase of $BiVO_4$ with lattice constants of $a=5.195$ Å, $b=11.70$ Å and $c=5.092$ Å (JCPDS card no. 14-0688). The morphology and structure of the as-obtained phase-pure $BiVO_4$ are characterized by scanning electron microscopy (SEM) and transmission electron microscopy (TEM), as shown in Figure 2. A panoramic SEM image shows that the $BiVO_4$ precursor consists of uniform discoid-like particles with a diameter of ca. 900 nm (Figure 2a). The magnified SEM images (Figure 2b,c) further reveal that these discoid-like particles possess smooth surface on the top and bottom, and rough surface composed of stacking nanosheets

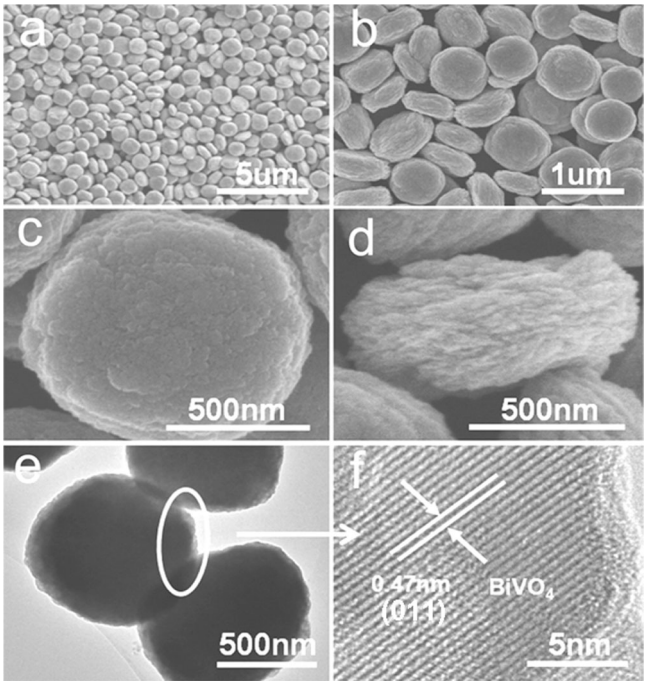

Figure 2. a–d) SEM, e) TEM and f) HRTEM images of the as-prepared $BiVO_4$ discoid-like particles.

on the lateral side. From the side view of a single discoid nanostructure (Figure 2d), the thickness is estimated to be ca. 300 nm for these discoid-like particles. TEM image (Figure 2e) further confirms the solid texture of these $BiVO_4$ particles. From the high-resolution (HR) TEM image (Figure 2f), the interplanar spacing of 0.47 nm can be well assigned to the (011) plane of the monoclinic $BiVO_4$ phase.

The hollow $BiVO_4/Bi_2S_3$ discoid heterostructures with a mesoporous shell are prepared by a facile anion exchange procedure under hydrothermal conditions using the $BiVO_4$ discoid-like particles as the precursor and Na_2S as the sulfidation agent. Due to the lower solubility of Bi_2S_3 relative to $BiVO_4$, the transformation of $BiVO_4$ into heterostructured $BiVO_4/Bi_2S_3$ is thermodynamically favored by reacting with S^{2-} anions. The successful formation of $BiVO_4/Bi_2S_3$ heterostructures is confirmed by XRD analysis (Figure S1, see SI). For products obtained with different Na_2S concentrations in the anion exchange reaction, in addition to the diffraction peaks of $BiVO_4$, other peaks can be well assigned to orthorhombic phase of Bi_2S_3 (JCPDS card no. 17-0320; $a=11.14$ Å, $b=11.30$ Å and $c=3.981$ Å). With the increase of Na_2S concentration, the diffraction intensity of the Bi_2S_3 phase becomes stronger, indicating the increasing content of Bi_2S_3 in the formed $BiVO_4/Bi_2S_3$ heterostructure.

A representative sample of the as-prepared $BiVO_4/Bi_2S_3$ heterostructures (sample H-3) is subjected to detailed characterizations. As shown in Figure 3a, the shape of the precursor $BiVO_4$ discoid is well preserved and the particles are fully converted into porous heterostructures. Some broken particles (inset in Figure 3a) clearly reveal the hollow feature of the $BiVO_4/Bi_2S_3$ heterostructures. Figure 3b shows the rough surface of the as-obtained heterostructures and the disordered wormhole-like pores throughout the particles. The hollow interior and detailed geometrical structure of the as-prepared $BiVO_4/Bi_2S_3$ heterostructures are directly elucidated by TEM observation. Figure 3c shows that the product well duplicates the size and shape of the $BiVO_4$ precursor particles, and the solid $BiVO_4$ discoid particles are fully converted into porous hollow heterostructures. It is anticipated that the initial anion exchange reaction during the hydrothermal treatment generates a thin Bi_2S_3 layer around the $BiVO_4$ surface. Subsequent anion exchange between $BiVO_4$ and S^{2-} ions leads to formation of hollow heterostructures with a mesoporous shell. The formation of hollow structure is likely due to the faster outward diffusion rate of Bi^{3+} cations than the inward diffusion rate of S^{2-} anions, which leads to the evacuation of Bi^{3+} in the inner region and thus generates the hollow interior.[25] It is also found that the hydrothermal reaction temperature has an important effect on the formation of mesoporous $BiVO_4/Bi_2S_3$ hollow heteronanostructures. When the hydrothermal reaction is carried out at 110 °C or 130 °C, no obviously porous $BiVO_4/Bi_2S_3$ heterostructures are formed (Figure S2, see SI). The formation of porous $BiVO_4/Bi_2S_3$ heterostructures is only observed at a higher temperature of 150 °C. It is presumed that the enhanced diffusion rate of VO_4^{3-} and S^{2-} at a higher reaction temperature favors the anion exchange reaction to form porous structures.

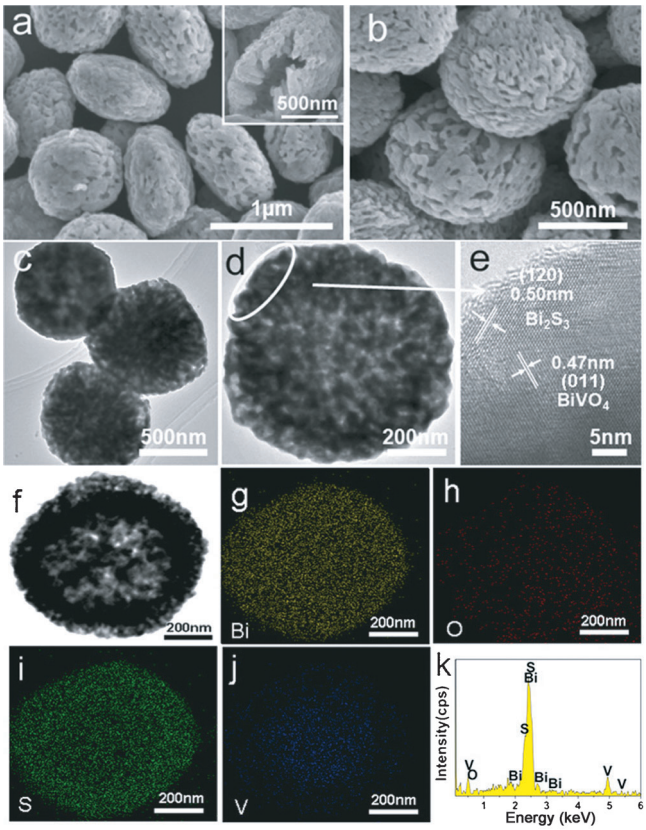

Figure 3. a,b) SEM, c,d) TEM and e) HRTEM images of the as-obtained mesoporous $BiVO_4/Bi_2S_3$ hollow discoids (sample H-3). The inset in (a) shows a broken hollow discoid. f) STEM image of a single representative $BiVO_4/Bi_2S_3$ hollow discoid (sample H-3) and the corresponding elemental mappings of g) Bi, h) O, i) S, and j) V elements, and k) EDX analysis.

A magnified TEM image of a single hollow particle (Figure 3d) confirms that the heterostructure is composed of numerous primary nanoparticles of tens of nm in size. The co-existence of both Bi_2S_3 and $BiVO_4$ phases and the hetero-junction region between them are clearly shown in the HRTEM image (Figure 3e). To reveal the spatial distribution of the two phases in the heterostructure, elemental mapping is performed on a single $BiVO_4/Bi_2S_3$ particle. As shown in Figure 3 f–k, the mapping result shows uniform distribution of Bi, V, O and S elements throughout the $BiVO_4/Bi_2S_3$ heterostructure. The S/V atomic ratio determined by energy dispersive X-ray spectroscopy (EDX) analysis is around 3.2, corresponding to a $BiVO_4/Bi_2S_3$ molar ratio of ca. 0.94 in the heterostructure. The EDX analysis (Table S1, see SI) also indicates that the $BiVO_4/Bi_2S_3$ molar ratio in the hetero-structures decreases when the concentration of Na_2S in the solution increases, which is consistent with the result of XRD analysis. The products with different $BiVO_4/Bi_2S_3$ molar ratios show similar discoid-like shape, but different porosity and roughness on the surface (Figure S3, see SI).

N_2 adsorption–desorption measurement is employed to further characterize the porous structure of the as-prepared heterostructures. The N_2 adsorption–desorption isotherm (Figure S4a, see SI) of the $BiVO_4/Bi_2S_3$ hollow heterostructure can be classified as type IV isotherm with a distinct hysteresis loop, indicating the existence of abundant mesopores in the particles.[38,39] Due to the relatively large size of the primary nanoparticles in the heterostructure, the sample H-3 exhibits only a moderate Brunauer–Emmett–Teller (BET) specific surface area of about 16.2 $m^2 g^{-1}$. Meanwhile, the Barrett–Joyner–Halenda (BJH) pore size distribution curve (Figure S4b, see SI) shows that the size of mesopores is centered around 10 nm. These mesoporous channels are anticipated to improve the photocatalytic activity by facilitating the diffusion of pollutants into the heterostructured particles.

The optical properties of as-prepared $BiVO_4/Bi_2S_3$ heterostructures are investigated. The UV/Vis diffuse reflectance spectra of $BiVO_4/Bi_2S_3$ heterostructures exhibit the same absorption band covering broader visible-light region than that of pure $BiVO_4$ (Figure S5a, see SI). The pure $BiVO_4$ has an absorption onset at 610 nm (Figure S5b, see SI), which corresponds to a band gap of 2.03 eV. The absorption edge of the $BiVO_4/Bi_2S_3$ heterostructures shows a red-shift toward the visible region. The representative $BiVO_4/Bi_2S_3$ heterostructure sample (sample H-3) exhibits a band gap of approximately 1.3 eV. This observation indicates that the $BiVO_4/Bi_2S_3$ heterostructures can be excited to generate more electron–hole pairs under visible-light irradiation, which might lead to enhanced photocatalytic activity.

The photocurrent transient response measurement of pure $BiVO_4$ and $BiVO_4/Bi_2S_3$ heterostructure (sample H-3) is performed. Figure 4 shows the rapid and consistent photocurrent responses for each switch-on and -off event in multiple 40 s on–off cycles under visible-light illumination. It is worth to note that the photocurrent density of the $BiVO_4/Bi_2S_3$ heterostructure electrode (ca. 23–40 μA cm^{-2}) is about one order of magnitude higher than that of the pure $BiVO_4$ electrode (ca. 2–4 μA cm^{-2}). The enhanced photocurrent response of the as-prepared mesoporous $BiVO_4/Bi_2S_3$

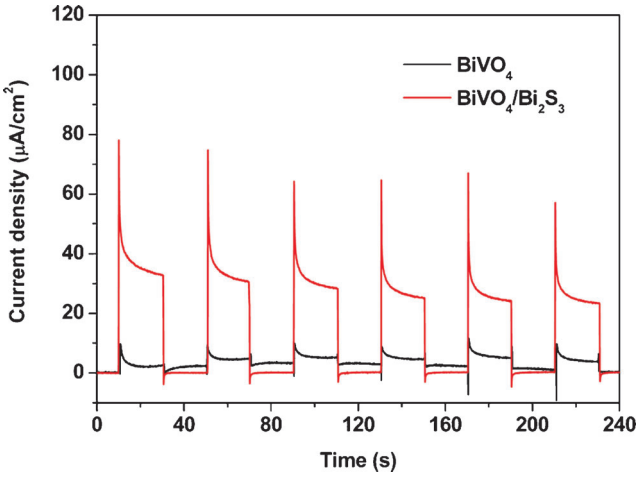

Figure 4. Photocurrent response of the as-prepared pure $BiVO_4$ discoids and heterostructured $BiVO_4/Bi_2S_3$ hollow discoids (sample H-3) under visible-light illumination. The electrodes are annealed at 350 °C in Ar for 1 h.

hollow heterostructures indicates higher separation efficiency of the photoinduced electron–hole pairs and a lower recombination rate in such hybrid structures under visible-light illumination.[41] This can be explained by the favorable transfer of electrons from Bi_2S_3 to $BiVO_4$ that reduces the recombination of electron–hole pairs as discussed shortly. Therefore, the $BiVO_4/Bi_2S_3$ heterostructures could be promising for photoelectrochemical energy conversion devices.

To demonstrate the photocatalytic activity of these unique mesoporous $BiVO_4/Bi_2S_3$ hollow heterostructures, photocatalytic reduction of Cr^{VI} by the as-obtained pure $BiVO_4$ and various $BiVO_4/Bi_2S_3$ heterostructure samples under visible-light irradiation is investigated as shown in Figure 5a. The sample H-3 exhibits the highest photocatalytic activity with 91.2% of Cr^{VI} degraded after irradiation for 60 min. Meanwhile, other heterostructures show slightly lower activity, which is still significantly higher than that of the pure $BiVO_4$ sample. This superior photocatalytic performance could be explained as follows. According to the band energy, the potentials of conduction band (CB) and valence band (VB) of Bi_2S_3 are more negative than that of $BiVO_4$ (Figure S6, see SI). Under visible-light irradiation, photogenerated electrons in the CB of Bi_2S_3 transfer to the CB of $BiVO_4$, while holes transfer in the opposite direction in the VB. The spontaneous transfer of electrons and holes in the $BiVO_4/Bi_2S_3$ heterostructure increases both the yield and lifetime of charge carriers by separating the photo-induced charges and reducing the chance for their recombination, which therefore enhances the photocatalytic performance. However, excessive Bi_2S_3 in the heterostructures might reduce the amount of photo-generated charges due to the unfavorable morphology and poor charge transport in Bi_2S_3.[42] In this particular case, the sample H-3 possesses the optimal charge separation and transport characteristics, thus demonstrating the highest photocatalytic activity. The photocatalytic activity for Cr^{VI} reduction is considered very high compared with previously reported $BiVO_4$ and other photocatalysts (Table S2, see SI). We have further studied the stability and reusability of the as-prepared heterostructures (sample H-3) by collecting and reusing the same photocatalyst for 6 cycles (Figure 5b). Only insignificant loss in photocatalytic activity is observed, which might be partly caused by incomplete collection of the photocatalyst during each step. The XRD pattern (Figure S7, see SI) of sample H-3 after the photocatalytic measurement reveals almost no deterioration in the crystal structure.

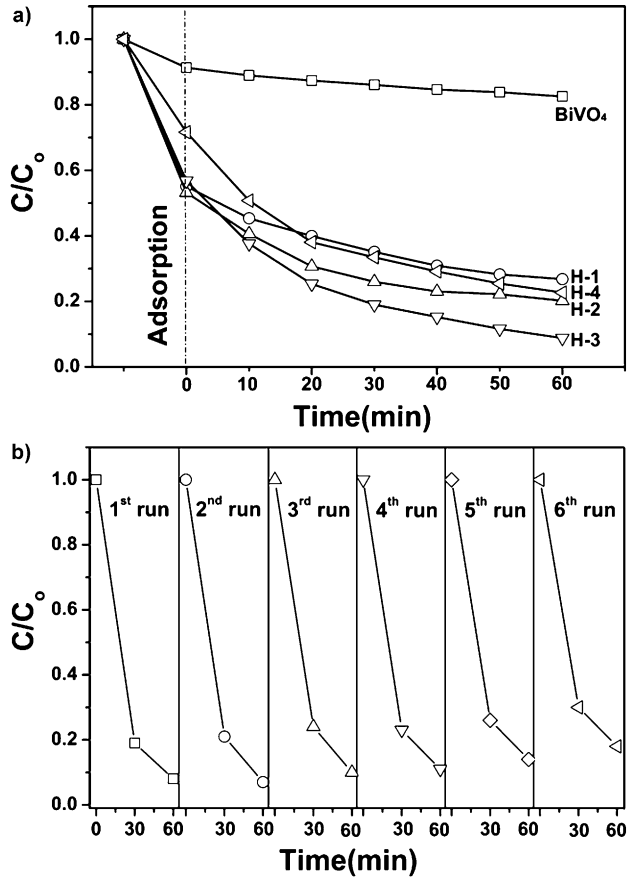

Figure 5. a) Photocatalytic reduction of Cr^{VI} in the presence of different photocatalysts under visible-light irradiation. b) 6 cycles of the photocatalytic reduction of Cr^{VI} using sample H-3 as the photocatalyst under visible-light irradiation for 60 min.

In summary, we have synthesized novel heterostructured $BiVO_4/Bi_2S_3$ hollow nano-discoids with mesoporous shell by a facile anion exchange approach. Uniform $BiVO_4$ discoid-like particles are first synthesized, and subsequently undergone chemical transformation in Na_2S solution under hydrothermal conditions. The formation of hollow heterostructures with mesoporous shell could be ascribed to the controlled anion exchange process. Importantly, the content of Bi_2S_3 in the $BiVO_4/Bi_2S_3$ heterostructures can be easily tuned by varying the concentration of Na_2S in the solution. As expected, the as-obtained heterostructured $BiVO_4/Bi_2S_3$ hollow discoids exhibit superior photocurrent response and photocatalytic activity for reduction of Cr^{VI} under visible-light illumination. This work will likely inspire further exploration for unconventional heteronanostructures with high potential for photocatlytic and optoelectronic applications.

Received: March 24, 2014
Published online: May 12, 2014

Keywords: energy conversion · mesoporous materials · photoelectrochemistry · semiconductors

[1] W. Wu, S. F. Zhang, F. Ren, X. H. Xiao, J. Zhou, C. Z. Jiang, *Nanoscale* **2011**, *3*, 4676.
[2] M. Saruyama, Y. G. So, K. Kimoto, S. Taguchi, Y. Kanemitsu, T. Teranishi, *J. Am. Chem. Soc.* **2011**, *133*, 17598.
[3] N. N. Hewa-Kasakarage, M. Kirsanova, A. Nemchinov, N. Schmall, P. Z. El-Khoury, T. A. N. Arnovsky, M. Zamkov, *J. Am. Chem. Soc.* **2009**, *131*, 1328.
[4] Y. Nonoguchi, T. Nakashima, T. Kawai, *small* **2009**, *5*, 2403.
[5] Y. Liu, L. Yu, Y. Hu, C. F. Guo, F. M. Zhang, X. W. Lou, *Nanoscale* **2012**, *4*, 183.
[6] Y. Hu, H. H. Qian, Y. Liu, G. H. Du, F. M. Zhang, L. B. Wang, X. Hu, *CrystEngComm* **2011**, *13*, 3438.
[7] L. Y. Mao, Y. R. Wang, Y. J. Zhong, J. Q. Ning, Y. Hu, *J. Mater. Chem. A* **2013**, *1*, 8101.

[8] W. L. Yang, L. Zhang, Y. Hu, Y. J. Zhong, H. B. Wu, X. W. Lou, *Angew. Chem.* **2012**, *124*, 11669; *Angew. Chem. Int. Ed.* **2012**, *51*, 11501.

[9] W. L. Yang, Y. Liu, Y. Hu, M. J. Zhou, H. S. Qian, *J. Mater. Chem.* **2012**, *22*, 13895.

[10] W. Wu, S. F. Zhang, X. H. Xiao, J. Zhou, F. Ren, L. L. Sun, C. Z. Jiang, *ACS Appl. Mater. Interfaces* **2012**, *4*, 3602.

[11] L. Zhang, L. Zhou, H. B. Wu, R. Xu, X. W. Lou, *Angew. Chem.* **2012**, *124*, 7379; *Angew. Chem. Int. Ed.* **2012**, *51*, 7267.

[12] X. Y. Zhou, J. J. Tang, J. Yang, J. Xie, L. L. Ma, *Electrochim. Acta* **2013**, *87*, 663.

[13] X. W. Lou, L. A. Archer, Z. C. Yang, *Adv. Mater.* **2008**, *20*, 3987.

[14] Y. J. Hwang, A. Boukai, P. D. Yang, *Nano Lett.* **2009**, *9*, 410.

[15] D. H. Son, S. M. Hughes, Y. D. Yin, A. P. Alivisatos, *Science* **2004**, *306*, 1009.

[16] L. Dloczik, R. Könenkamp, *Nano Lett.* **2003**, *3*, 651.

[17] R. D. Robinson, B. Sadtler, D. O. Demchenko, C. K. Erdonmez, L. W. Wang, A. P. Alivisatos, *Science* **2007**, *317*, 355.

[18] M. V. Kovalenko, D. V. Talapin, M. A. Loi, F. Cordella, G. Hesser, M. I. Bodnarchuk, W. Heiss, *Angew. Chem.* **2008**, *120*, 3071; *Angew. Chem. Int. Ed.* **2008**, *47*, 3029.

[19] B. Sadtler, D. O. Demchenko, H. M. Zheng, S. M. Hughes, M. G. Merkle, U. Dahmen, L. W. Wang, A. P. Alivisatos, *J. Am. Chem. Soc.* **2009**, *131*, 5285.

[20] S. L. Xiong, H. C. Zeng, *Angew. Chem.* **2012**, *124*, 973; *Angew. Chem. Int. Ed.* **2012**, *51*, 949.

[21] H. F. Cheng, B. B. Huang, Y. Y. Liu, Z. Y. Wang, X. Y. Qin, X. Y. Zhang, Y. Dai, *Chem. Commun.* **2012**, *48*, 9729.

[22] Y. D. Yin, R. M. Rioux, C. K. Erdonmez, S. Hughes, G. A. Somorjai, A. P. Alivisatos, *Science* **2004**, *304*, 711.

[23] H. L. Cao, X. F. Qian, C. Wang, X. D. Ma, J. Yin, Z. K. Zhu, *J. Am. Chem. Soc.* **2005**, *127*, 16024.

[24] J. N. Gao, Q. S. Li, H. B. Zhao, L. S. Li, C. L. Liu, Q. H. Gong, L. M. Qi, *Chem. Mater.* **2008**, *20*, 6263.

[25] J. Park, H. M. Zheng, Y. W. Jun, A. P. Alivisatos, *J. Am. Chem. Soc.* **2009**, *131*, 13943.

[26] L. I. Hung, C. K. Tsung, W. Y. Huang, P. D. Yang, *Adv. Mater.* **2010**, *22*, 1910.

[27] M. L. Pang, H. C. Zeng, *Langmuir* **2010**, *26*, 5963.

[28] C. H. Kuo, Y. T. Chu, Y. F. Song, M. H. Huang, *Adv. Funct. Mater.* **2011**, *21*, 792.

[29] A. Kudo, K. Omori, H. Kato, *J. Am. Chem. Soc.* **1999**, *121*, 11459.

[30] W. J. Jo, J. W. Jang, K. J. Kong, H. J. Kang, J. Y. Kim, H. Jun, K. P. S. Parmar, J. S. Lee, *Angew. Chem.* **2012**, *124*, 3201; *Angew. Chem. Int. Ed.* **2012**, *51*, 3147.

[31] S. Kohtani, M. Koshiko, A. Kudo, K. Tokumura, Y. Ishigaki, A. Toriba, K. Hayakawa, R. Nakagaki, *Appl. Catal. B* **2003**, *46*, 573.

[32] M. Zhou, H. B. Wu, J. Bao, L. Liang, X. W. Lou, Y. Xie, *Angew. Chem.* **2013**, *125*, 8741 – 8745; *Angew. Chem. Int. Ed.* **2013**, *52*, 8579.

[33] S. J. Hong, S. Lee, J. S. Jang, J. S. Lee, *Energy Environ. Sci.* **2011**, *4*, 1781.

[34] D. K. Ma, M. L. Guan, S. S. Liu, Y. Q. Zhang, C. W. Zhang, Y. X. He, S. M. Huang, *Dalton Trans.* **2012**, *41*, 5581.

[35] X. F. Zhang, Y. Gong, X. L. Dong, X. X. Zhang, C. Ma, F. Shi, *Mater. Chem. Phys.* **2012**, *136*, 472.

[36] S. Balachandran, M. K. Swaminathan, *Dalton Trans.* **2013**, *42*, 5338.

[37] Z. Q. Li, X. S. Lin, L. Zhang, X. T. Chen, Z. L. Xue, *CrystEngComm* **2012**, *14*, 3495.

[38] X. F. Zhou, Z. L. Hu, Y. Q. Fan, S. Chen, W. P. Ding, N. P. Xu, *J. Phys. Chem. C* **2008**, *112*, 11722.

[39] M. Kruk, M. Jaroniec, *Chem. Mater.* **2001**, *13*, 3169.

[40] M. C. Long, W. M. Cai, J. Cai, B. X. Zhou, X. Y. Chai, Y. H. Wu, *J. Phys. Chem. B* **2006**, *110*, 20211.

[41] Q. P. Luo, X. Y. Yu, B. X. Lei, H. Y. Chen, D. B. Kuang, C. Y. Su, *J. Phys. Chem. C* **2012**, *116*, 8111.

[42] J. Kim, M. Kang, *Int. J. Hydrogen Energy* **2012**, *37*, 8249 – 8256.

